Table of Contents

List of figures

i

List of tables

Nomenclature

DRR	Desalination rate ratio [-]		*Greek letters*	
$\dot{E}x$	Exergy [W]	η	Efficiency [%]	
e	Flow exergy [J/kg]	μ	Chemical potential [J/kg]	
G	Gibbs energy [J]	ω	Humidity ratio [kg/kg]	
g	Specific Gibbs energy [J/kg]	Δ	Drop [-]	
GOR	Gain Output Ratio [-]			
h	Specific enthalpy [J/kg]		*Subscripts*	
h_{fg}	Latent heat of evaporation [J/kg]	a	Air	
$\dot{m}$	Mass flow rate [kg/h]	b	Brine	
$MFRR$	Mass flow rate ratio [-]	dw	Desalinated water	
P	Pressure [Pa]	mc	M-cycle	
$\dot{Q}$	Heat supplied [W]	sw	Saline water	
R	Gas constant [J/kg/K]	swh	Saline water heater	
RR	Recovery ratio [-]	swp	Saline water pump	
s	Specific entropy [J/kg/K]	w	Pure water	
$\dot{S}_{gen}$	Entropy generation rate [W/K]	t	Total	
Sl	Salinity [g/kg]	0	Dead state	
SR	Salinity ratio [-]	1,2,3,4,5,6,	State points	
		7,8,9		
SEC	Specific energy consumption [kWh/kg]	12	Dry air channel	
t	Temperature [°C]	23	Humidification air channel	
T	Temperature [K]	34	Dehumidification air channel	
$\dot{V}$	Volume flow rate [m³/s]		*Abbreviations*	
$\dot{W}$	Work [W]	HDD	Humidification-dehumidification desalination	
w_s	Salinity [kg/kg]	$M-cycle$	Maisotsenko cycle	
x	Mass Fraction [-]	$OAOW$	Open air open water	

The Second Law analysis of a humidification-dehumidification desalination system using M-cycle

Mansoor Abdul Aziz[1,*], Jie Lin[2], František Mikšík[1,3], Takahiko Miyazaki[1,3], Kyaw Thu[1,3]

[1] Department of Advanced Environmental Science and Engineering, Faculty of
Engineering Sciences, Kyushu University
Kasuga-koen 6-1, Kasuga-city, Fukuoka 816-8580, Japan
[2] Department of Engineering Science, University of Oxford
Parks Road, Oxford OX1 3PJ, United Kingdom
[3] Thermal Science and Engineering Division, International Institute of Carbon-Neutral
Energy Research (I2CNER), Kyushu University
744 Motooka, Nishi-ku, Fukuoka 819-0395, Japan

* Corresponding author's email: aziz.mansoor.435@s.kyushu-u.ac.jp (M. Abdul Aziz)

Abstract

Humidification-dehumidification desalination (HDD) systems offer a feasible approach for the production of fresh water in inaccessible areas as they can be operational using renewable energy and require little maintenance. Various studies are being carried out to boost the system performance. In this paper, an open air open water HDD system is proposed that exploits the enhanced evaporation and condensation processes by implementing with the Maisotsenko cycle (M-cycle). The system utilizes solar energy as the energy input to heat the saline water. A thermodynamic model is formulated under steady-state conditions, considering the first and second law of thermodynamics. The energetic and exergetic performance of the system is studied. The model is first validated with the experimental data and a good agreement is found where the maximum discrepancy is about 6.0 %. Effects of different operating conditions on key performance parameters such as the Gain Output Ratio (GOR), specific energy consumption (SEC), exergy destruction, and exergy efficiency are analyzed. An improvement is observed in the GOR when the inlet air temperature is raised at constant humidity ratio. The system exhibits better performance in dry air environment when compared with humid air environment. The analysis shows a maximum mass flow rate of desalinated water of 22.3 kg/h, recovery ratio (RR) of 0.223, GOR of 3, SEC of 0.23 kWh/kg and an exergy efficiency of 43.21 %.

Keywords: M-cycle; Humidification-dehumidification; Desalination; Exergy destruction; Exergy efficiency

Highlights

- Humidification-dehumidification desalination using M-cycle for improved performance
- Exploit the sub wet-bulb temperature cooling of M-cycle for condensation
- A comprehensive thermodynamic model for M-cycle based HDD is developed
- A detailed exergy analysis of the present system is conducted

1. Introduction

Water covers around 71% of the surface of the Earth, out of which almost 96.5% exists as saline water and the rest exists as freshwater [1]. Two-thirds of the freshwater is not readily available as it occurs in the form of snow, ice, glaciers, and others [2]. There has been a considerable rise in the demand of freshwater due to the increase in population and it is assessed that approximately five billion people will suffer from water scarcity by 2050 [3,4]. Hence, desalination, as a method of obtaining potable water by eliminating salts from saline water, is a practical answer to tackle the problem of water shortage [5].

Desalination systems are broadly classified into two groups: (a) thermal-driven like vapor compression (VC), multi-stage flash (MSF), multi-effect distillation (MED), membrane distillation (MD), humidification-dehumidification desalination (HDD), solar still, adsorption desalination (AD), and (b) mechanical-driven like electrodialysis (ED) and reverse osmosis (RO) [6]. Humidification-dehumidification desalination (HDD) works on the principle of a rain cycle, converting saline water to potable water by using air as the carrier gas [7]. HDD systems are appropriate for small scale and non-grid applications as they have a simple construction and in comparison to MSF, MED and RO systems they are easier to maintain [8].

HDD systems can be divided into two categories. In the first category, based on the heating fluid, they are divided into water-heated systems [9] and air-heated systems [10]. In the second category, based on fluid flow arrangements, they are subdivided into four: closed water open air systems (CWOA) [11,12], closed air open water systems (CAOW) [13,14], open air open water systems (OAOW) [15,16], and closed water closed air systems (CWCA) [17,18]. Khalil et al. [11] performed an experiment which analyzed a water-heated CWOA HDD system with bubble column humidifier, and the dehumidifier being shell and tube heat exchanger. They observed better performance with bubble column humidifier as

compared to direct sprayed humidifier with 21 kg/day of yield and 0.53 as the Gain Output Ratio (GOR). Abd-ur-Rehman et al. [12] also conducted an experimental analysis of water-heated CWOA HDD system with multi-stage bubble column humidifier. They concluded that, for air leaving the humidifier, the humidity ratio was 7-9% greater for two-stage humidifier and 18-21% greater for three-stage humidifier in comparison with the single stage humidifier, which resulted in better performance. Narayan et al. [13] carried out an experiment which investigated a CAOW HDD system and they reported a GOR of 4 and 700 kg/day rate of fresh water output. Rahimi-Ahar et al. [14] performed an experiment which studied a CAOW HDD system with sub-atmospheric packed-bed direct water spray humidifier. The dehumidifier used was double pipe heat exchanger. The authors noted a GOR of 3.43 and a yield of 1.07 $kg/h/m^2$. Kabeel et al. [15] conducted an experiment that analyzed an OAOW HDD system with packed-bed humidifier and a GOR of 1.79 and 42.3 kg/day rate of fresh water production was observed. They also concluded that higher mass flow rate of air enhanced the production of freshwater. An experimental work was carried out by Zubair et al. [16] of OAOW and CWOA HDD system with three stage cellulose pads as humidifier. They noted a GOR of 1.6 in case of CWOA HDD system, which performed better than OAOW HDD system due to the heat recovery of brine. Behnam et al. [17] conducted an experimental analysis of CWCA HDD system with bubble column humidifier and 6.275 $kg/day/m^2$ rate of fresh water yield and a GOR of 0.65 were reported. An experimental study of CWCA HDD system was performed by Nafey et al. [18] with a packed-bed humidifier and a yield of 10.25 kg/day was observed.

Although several experimental and theoretical research works have been carried out on HDD systems for more than two decades, Narayan et al. [19] were the first to introduce the thermodynamic model for water-heated CWOA and CAOW HDD systems. They concluded that both configurations showed similar

performance (GOR ≈ 2.5). Replacing the former systems with the air-heated design, the performance dropped significantly (GOR ≈ 0.78). They also proposed several modifications in the HDD systems to increase the performance. Mistry et al. [20,21] performed the second law analyses of CAOW and OAOW HDD systems. They concluded that for the water-heated case, OAOW performed better than CAOW HDD system irrespective of the ambient relative humidity. In case of the air-heated approach, CAOW performed better than OAOW HDD system. They further concluded that when the mass flow rate ratio is varied, the performance could reach its peak as the total entropy generation of the cycle is minimized. The thermodynamic performance of a water-heated OAOW HDD system made up of a packed-bed humidifier and dehumidifier was examined by He et al. [22]. They reported that the best desalination performance was observed at GOR equal to 1.7 and 96.45 of kg/h water production. Xu et al. [23] performed a thermodynamic study of water-heated CWCA HDD system with an evaporative condenser. They showed that the maximum performance was achieved at GOR equal to 12.24, 0.14 kg/h water production and specific energy consumption (SEC) equal to 18.35 kg/kWh.

Maisotsenko cycle (M-cycle) is a thermodynamically based technique that employs energy accessible from the latent heat of water vaporizing into the air. This psychrometric renewable energy is then exploited to collect energy from the air. Using the M-cycle, the air temperature can be reduced to the dew-point temperature while many experimental evidences exhibit that the product air temperature is lower than the wet-bulb temperature. Hence, it is also an advanced indirect evaporative cooling (IEC) process. Saturated hot air can also be a by-product of the M-cycle, making it a process by which heat can be recovered and consequently, system efficiency can be improved for numerous applications [24]. Several exergy analyses of the M-cycle coolers have been carried out. For example, Dizaji et al. [25] studied the M-cycle cooler, they concluded that the

exergy efficiency declines when temperature of inlet air is raised and improves when the humidity ratio of inlet air is raised. Lin et al. [26] conducted an in-depth investigation of an M-cycle based counter-flow dew point evaporative cooler. They reported that the exergy efficiency increased when the temperature of inlet air was raised from 25°C to 30°C and then remained almost constant till 45°C when the humidity ratio of inlet air was kept constant. When the inlet air temperature was kept constant, higher inlet air humidity ratio led to a decrease in exergy efficiency.

While the M-cycle is extensively investigated for cooling, its key water evaporation process has made it favorable for desalination through combination with existing desalination systems [27]. Chen et al. [28] presented an experimental work on the integrated IEC-HDD cycle for cooling as well as freshwater production using a conventional M-cycle. They concluded that under the same operating conditions, the observed rate of freshwater production of 25-125 L/h and GOR of 1.6–2.5 was greater than other HDD configurations. Tariq et al. [29] analyzed the HDD system with M-cycle based humidifier (air saturator), they inferred that this system performed better as opposed to the HDD system with the direct contact humidifier. Recently, a water desalination system consisting of M-cycle arranged in two and three stages, respectively, was proposed by Pandelidis et al. [30]. They noted that while the three-stage system showed better performance than the two-stage system, the two-stage system showed better SEC under the same operating conditions. Chudnovsky et al. [31] implemented a water distillation system based on indirect dew point evaporation system. The arrangement of the system is similar to CWOA HDD system using M-cycle with three air channels i.e., dry, evaporation and condensation channels respectively. Table 1 summarizes the comparison between the current study and previously studied M-cycle based HDD systems.

Thus far, previous studies have included research on integration of M-cycle with conventional HDD system for cooling and desalination [28], replacement of direct contact humidifier with M-cycle based humidifier in a standard HDD system [29], multi-stage M-cycle based desalination system [30]. These systems have used M-cycle comprising of two distinct air channels i.e., dry and wet channels respectively. However, there has been very few research on HDD systems using M-cycle comprising of three different air channels. The existing work [31] has focused on freshwater production rate, recovery ratio (RR), desalination rate ratio (DRR) but excluded important performance parameters like Gain Output Ratio (GOR) and specific energy consumption (SEC). The understanding of these latter mentioned parameters (GOR, SEC) is necessary to compete with current HDD systems and other thermal desalination systems.

In this paper, a water-heated open air open water (OAOW) HDD system using M-cycle is proposed. The M-cycle consists of three different types of air channels i.e., dry, humidification and dehumidification channels respectively. The use of three air channels in the system allows both humidification and dehumidification to take place in one component i.e., the M-cycle. The temperature of the air is lowered to below the wet-bulb temperature in the dry air channel, and then it flows into the humidification channel where the preheated saline water evaporates which increases the humidity of the air. This saturated humid air enters the dehumidification channel and condenses to give fresh water. The aim of this work is to implement the first and second law of thermodynamics to study the energetic and exergetic performance of the HDD system.

Table 1 Comparison between the present study and previous studies on M-cycle based HDD systems.

Study	Research technique	M-cycle	Features
Chen et al. [28]	Experiment, simulation	Used with regular HDD system	1. Employed for cooling and freshwater production 2. Improved performance when compared to other HDD systems
Tariq et al. [29]	Simulation	Used as humidifier	1. Fresh water production rate, recovery ratio, and GOR significantly improved when compared to direct contact humidifier-based HDD system 2. Works best in dry and hot climatic conditions
Pandelidis et al. [30]	Simulation	Used as HDD system	1. M-cycle arranged in two and three stages respectively 2. Three stage showed better performance 3. Energy consumption was less when compared with other desalination methods
Chudnovsky et al. [31]	Experiment	Used as HDD system	1. Experimental setup built by Idalex Inc. (USA) 2. Waste water was used for water distillation
Current study	Simulation	Used as HDD system	1. M-cycle comprises of three adjacent air channels 2. Extensive thermodynamic analysis is studied 3. Comprehensive exergy analysis is carried out

2. Description of M-cycle based HDD system

Figure 1 shows the proposed M-cycle based water-heated OAOW HDD system. It consists of an M-cycle, a solar water heater, a saline water pump and a saline water tank. The M-cycle consists of three types of channels i.e., dry channel, humidification (evaporating) channel, and dehumidification (condensing) channel. The state points 1, 2, 3, and 4 represent the air flow from inlet to exhaust undergoing humidification and dehumidification processes while producing potable water from the saltwater. Air enters at state point 1, passes through the dry channel, enters the humidification channel at state point 2, comes into contact with heated saline water, and humidifies the air at state point 3. Humid air then enters the dehumidification channel, where its moisture content condenses into liquid water and the desalinated water leaves at state point 9 while the exhaust air leaves at state point 4. Saline water from a tank at state point 5 is pumped to a solar water heater where it enters at state point 6 and is heated to a desired temperature at state point 7. Preheated saline water at state point 7 enters the humidification channel so that the air comes in contact with it to stimulate evaporation or humidification. At state point 8, salinity of the saline water increases which exits as brine. Eventually, the condensed water at state point 9 is obtained as the desalinated (fresh) water. Figure 2 presents a comprehensive illustration of the three different types of air channels used in the M-cycle along with the air and water flows respectively.

The psychrometric chart for the M-cycle is shown in Figure 3. The chart illustrates the three different air channel processes. In the dry channel process (1-2), where state point 1 is the ambient air temperature of 45 °C and relative humidity of 20 %, the ambient air is nearly cooled to the dew point temperature. The process of evaporation occurs in the humidification channel (2-3) which increases the humidity ratio. Finally, the saturated humid air condenses in the dehumidification channel (3-4).

3. Modeling of M-cycle based HDD system

A thermodynamic model is established for the water-heated OAOW HDD system (Figure 1), where the mass, energy, entropy and exergy balances are judiciously considered. The goal of this model is to study the energetic and exergetic performance of the system. The following assumptions are adopted in the current model:

i.   No heat loss from all components of the system [32].

ii. Steady state operation of the system.

iii. Humid air leaving the humidification channel is saturated i.e., relative humidity at state point 3 is 100% [33].

iv. Exhaust air leaving the dehumidification channel is saturated i.e., relative humidity at state point 4 is 100% [33].

v.   Desalinated water obtained at state point 9 has zero salinity i.e., pure water.

vi. Exhaust air temperature is equal to desalinated water temperature i.e., temperature at state point 4 is equal to temperature at state point 9.
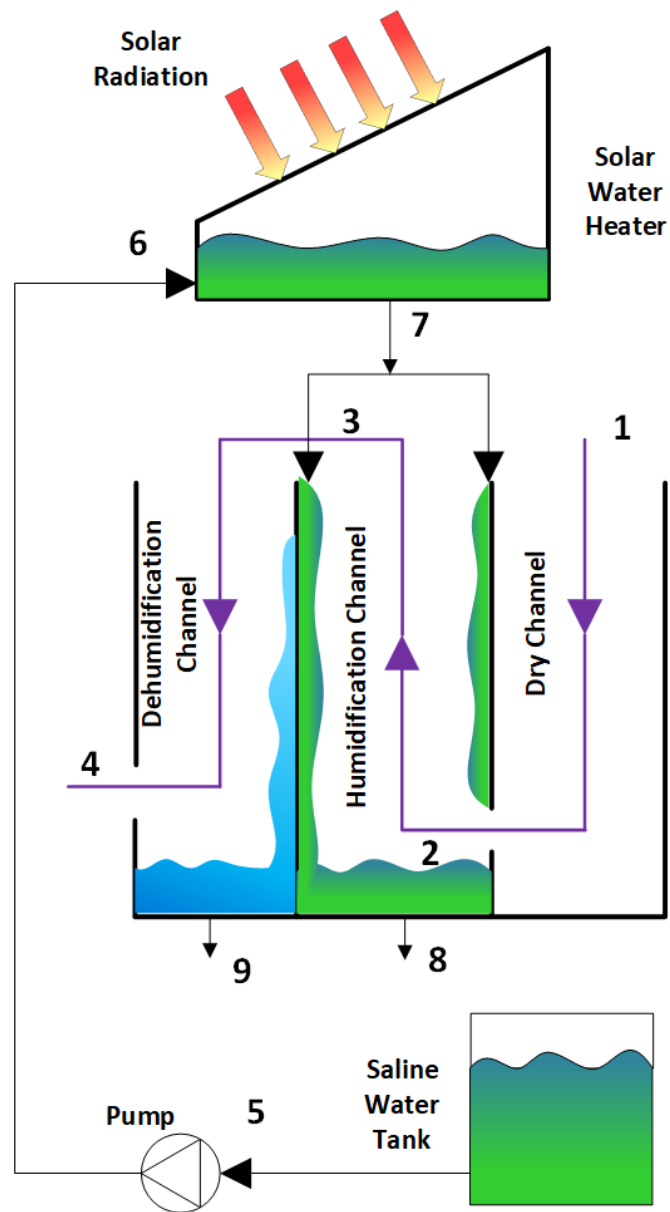
Figure 1 M-cycle based HDD system.
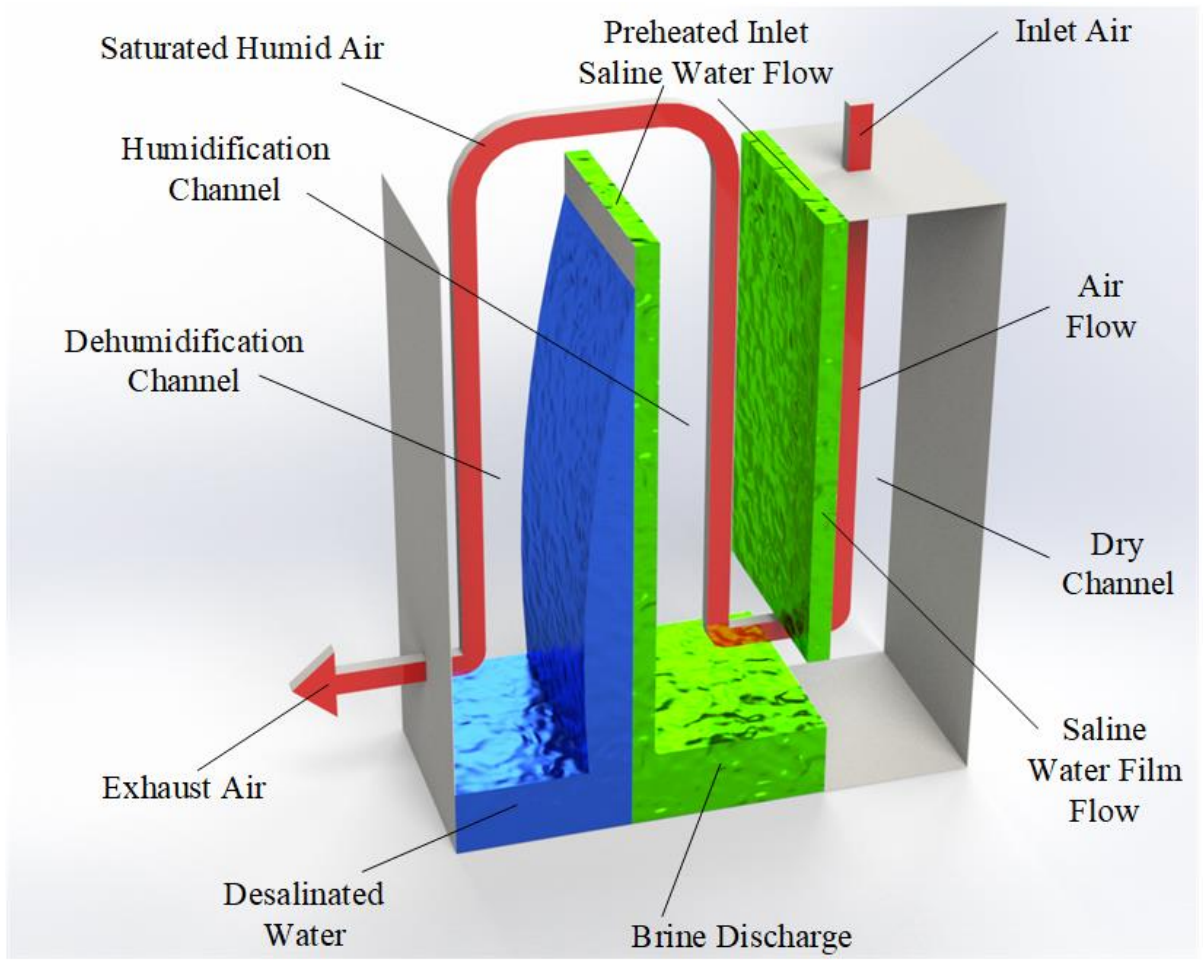
Figure 2 Schematic representation of the M-cycle used for the system.
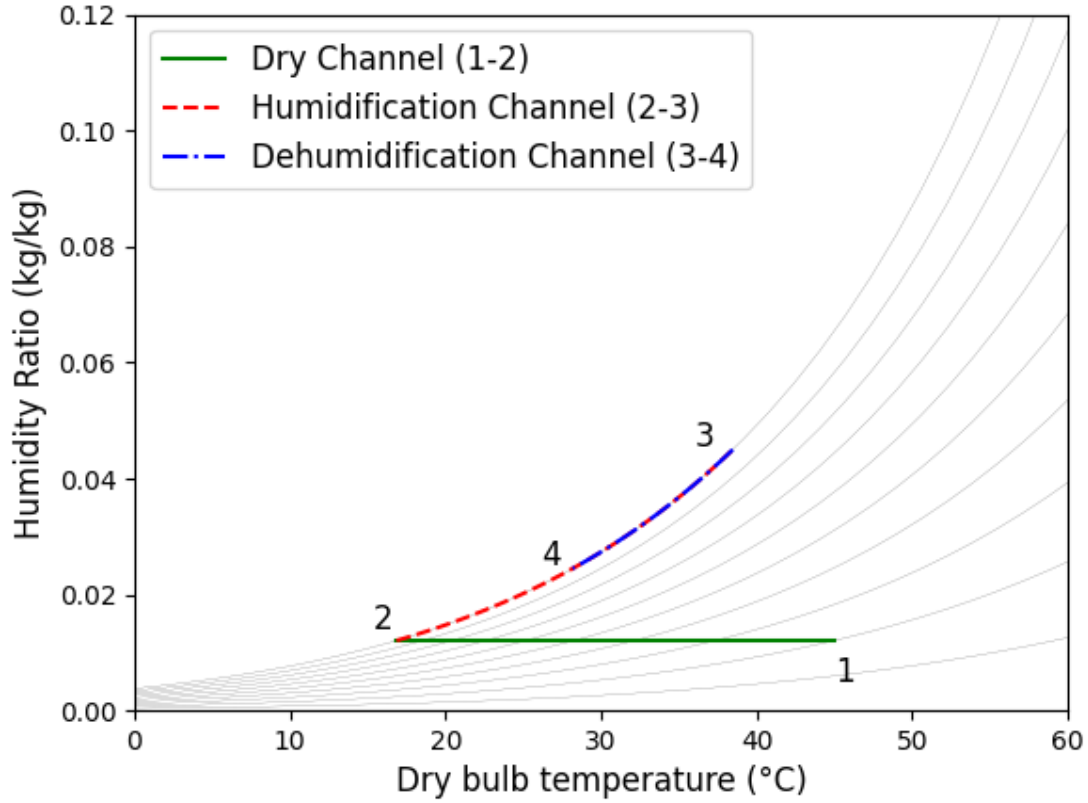
Figure 3 Psychrometric chart for M-cycle in an M-cycle based HDD system.

3.1 Mass, energy, and entropy balances

When taking M-cycle as the control volume, the general mass balance equations for water and salt can be expressed as:

$$\dot{m}_a \omega_1 + \dot{m}_{sw} = \dot{m}_b + \dot{m}_a \omega_4 + \dot{m}_{dw} \tag{1}$$

$$\dot{m}_{sw} Sl_{sw} = \dot{m}_b Sl_b \tag{2}$$

Here, $\dot{m}$ represents the mass flow rate and Sl denotes the salinity. Besides, if the dehumidification channel is taken as the control volume, an equation of mass balance for water can be written as:

$$\dot{m}_{dw} = \dot{m}_a(\omega_3 - \omega_4) \tag{3}$$

A mass flow rate ratio is introduced and it may be defined as the ratio of saline water mass flow rate to air mass flow rate.

13

$$MFRR = \frac{\dot{m}_{sw}}{\dot{m}_a} \tag{4}$$

Similarly, the salinity ratio is defined as the ratio of saline water salinity to brine salinity.

$$SR = \frac{Sl_{sw}}{Sl_b} \tag{5}$$

Rearranging equations (1) - (5) yields equation (6):

$$\omega_3 = \omega_1 + MFRR(1 - SR) \tag{6}$$

Similar to the mass balance, a general equation of energy balance for M-cycle is formulated as:

$$\dot{m}_a h_1 + \dot{m}_{sw} h_7 = \dot{m}_b h_8 + \dot{m}_a h_4 + \dot{m}_{dw} h_9 \tag{7}$$

The energy balance for the solar water heater is expressed as:

$$\dot{Q}_{swh} = \frac{\dot{m}_{sw}(h_7 - h_6)}{3600} \tag{8}$$

The work input of the saline water pump is written as:

$$\dot{W}_{swp} = \frac{\dot{m}_{sw}(h_6 - h_5)}{3600} \tag{9}$$

The fan power consumption of the M-cycle is written as:

$$\dot{W}_{fan} = \dot{V}_{12}\Delta P_{12} + \dot{V}_{23}\Delta P_{23} + \dot{V}_{34}\Delta P_{34} \tag{10}$$

After the mass and energy balances are defined, the input variables considered are inlet air temperature, inlet air humidity ratio, preheated inlet saline water temperature, inlet salinity of saline water, and MFRR. The temperature of humid air at the end of humidification channel, and brine temperature are also estimated. Subsequently, the exhaust air temperature, and desalinated water temperature are computed using the mass, and energy balances.

Furthermore, the entropy balance for M-cycle is written as:

$$\dot{S}_{gen,mc} = \left(\frac{\dot{m}_a s_4 + \dot{m}_b s_8 + \dot{m}_{dw} s_9 - \dot{m}_a s_1 - \dot{m}_{sw} s_7}{3600}\right) \tag{11}$$

The entropy balance for the solar water heater is written as:

$$\dot{S}_{gen,swh} = \left(\frac{\dot{m}_{sw} s_7 - \dot{m}_{sw} s_6}{3600}\right) - \frac{\dot{Q}_{swh}}{T_{swh}} \tag{12}$$

Hence, the total entropy generation rate is written as:

$$\dot{S}_{gen,t} = \dot{S}_{gen,mc} + \dot{S}_{gen,swh} \tag{13}$$

3.2 Performance parameters

The performance of an HDD system is given by Gain Output Ratio (GOR), written as:

$$GOR = \frac{\dot{m}_{dw} h_{fg}}{\left(\dot{Q}_{swh} + \dot{W}_{swp} + \dot{W}_{fan}\right) \times 3600} \tag{14}$$

The GOR is an estimate of the amount of desalinated water produced for a particular heat and/or work input.

The specific energy consumption (SEC) of an HDD system is given as:

$$SEC = \frac{\dot{Q}_{swh} + \dot{W}_{swp} + \dot{W}_{fan}}{1000 \times \dot{m}_{dw}} \tag{15}$$

The SEC is a measure of energy used for producing a unit amount of desalinated water.

The recovery ratio (RR) is defined as the ratio of mass flow rate of desalinated water to mass flow rate of saline water.

$$RR = \frac{\dot{m}_{dw}}{\dot{m}_{sw}} \tag{16}$$

The RR is an estimate of the quantity of water recovered for a given amount of saline water.

The desalination rate ratio (DRR) is defined as the ratio of mass flow rate of desalinated water to mass flow rate of evaporation.

$$DRR = \frac{\dot{m}_{dw}}{\dot{m}_{evap}} = \frac{\dot{m}_{dw}}{\dot{m}_{sw} - \dot{m}_b} = \frac{\dot{m}_{dw}}{\dot{m}_{sw}(1 - SR)} \tag{17}$$

The DRR is a measure of condensate produced for a unit amount of vapor produced.

3.3 Exergy Analysis

The exergy balance for saline water heater is written as:

$$\frac{\dot{m}_{sw}e_6}{3600} + \dot{Q}_{swh}\left(1 - \frac{T_0}{T_{swh}}\right) = \frac{\dot{m}_{sw}e_7}{3600} + T_0\dot{S}_{gen,swh} \tag{18}$$

The exergy efficiency of the saline water heater is written as:

$$\eta_{ex,swh} = \frac{\dot{Ex}_{out,swh}}{\dot{Ex}_{in,swh}} \times 100 \tag{19}$$

The exergy balance for M-cycle is written as:

$$\frac{\dot{m}_a e_1 + \dot{m}_{sw}e_7}{3600} = \frac{\dot{m}_b e_8 + \dot{m}_a e_4 + \dot{m}_{dw}e_9}{3600} + T_0\dot{S}_{gen,mc} \tag{20}$$

The exergy efficiency of the M-cycle is expressed as:

$$\eta_{ex,mc} = \frac{\dot{Ex}_{out,mc}}{\dot{Ex}_{in,mc}} \times 100 \tag{21}$$

The total exergy balance for M-cycle based HDD system is written as:

$$\frac{\dot{m}_a e_1 + \dot{m}_{sw}e_6}{3600} + \dot{Q}_{swh}\left(1 - \frac{T_0}{T_{swh}}\right) = \frac{\dot{m}_b e_8 + \dot{m}_a e_4 + \dot{m}_{dw}e_9}{3600} + T_0\dot{S}_{gen,t} \tag{22}$$

The total exergy efficiency of the M-cycle based HDD system is written as:

$$\eta_{ex,total} = \frac{\dot{Ex}_{out,total}}{\dot{Ex}_{in,total}} \times 100 \qquad (23)$$

3.4 Exergy calculation procedure

Once the model has been established and the objective variables have been determined, the entropy generation rates of saline water heater, and M-cycle are calculated. Next, the performance parameters are computed and exergy parameters are evaluated. The calculation procedure flow chart is depicted in Figure 4.

3.5 Simulation conditions for exergy analysis

Numerical simulations based on the thermodynamic model were conducted to calculate the energetic and exergetic performance of the desalination system. Table 2 shows the various parameters and conditions along with their nominal values and ranges. Table 3 lists the dead state conditions for the exergy analysis. Gain Output Ratio (GOR), specific energy consumption, exergy destruction and exergy efficiency are the important objective parameters for this analysis. The results are presented and discussed in the coming sections.

Table 2 Simulation parameters for exergy analysis.

Parameter	Nominal value	Varying range
m_{sw} ($kg\ h^{-1}$)	100	100 - 200
m_a ($kg\ h^{-1}$)	1000	500 - 1000
t_1 (°C)	45	25 - 45
t_7 (°C)	60	40 - 60
Sl_{sw} ($g\ kg^{-1}$)	35	10 - 50
$\omega_1 \left(\dfrac{kg}{kg}\right)$	0.01	0.005 - 0.025
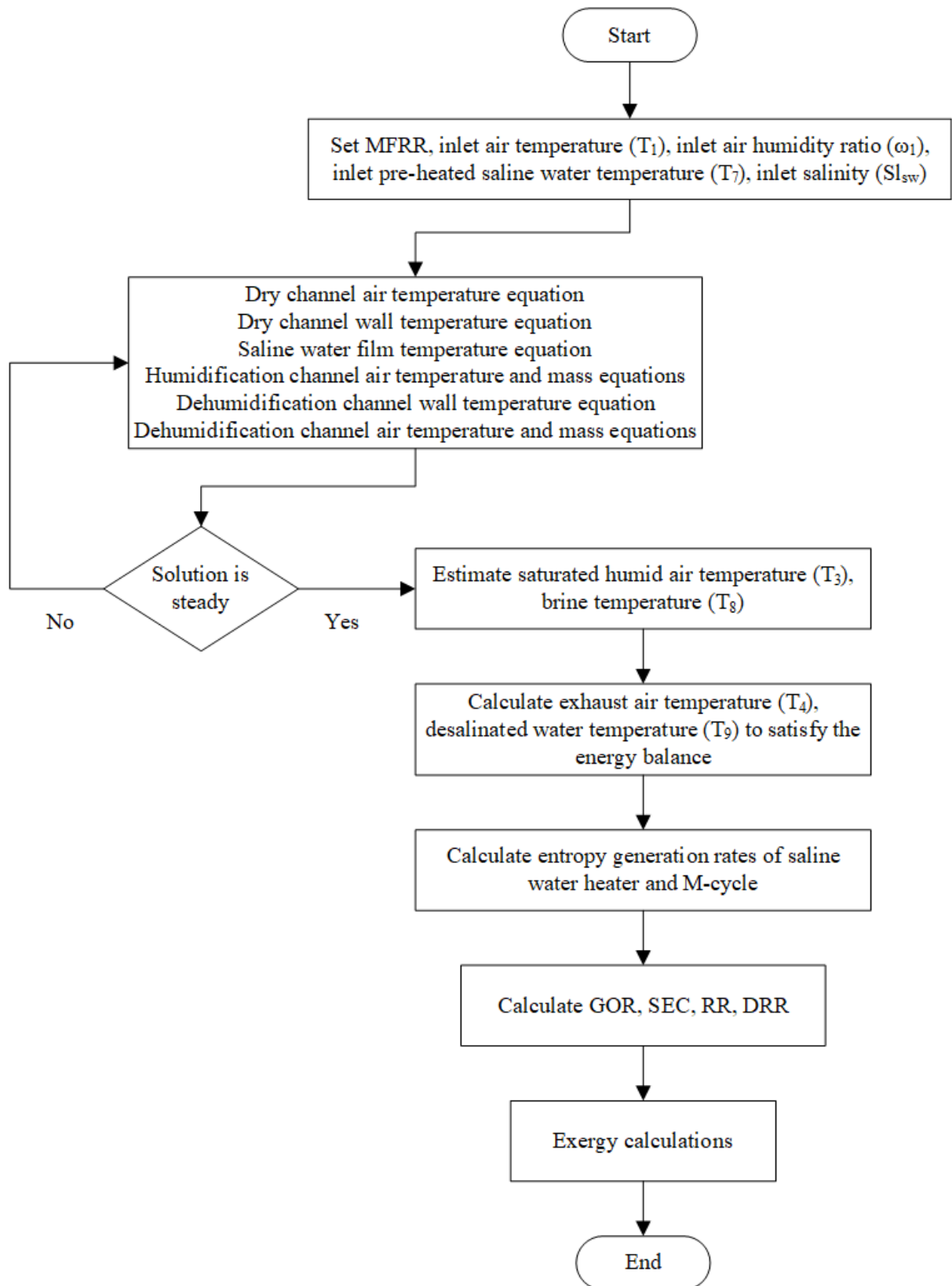
Figure 4 Exergy model calculation flow chart for M-cycle based HDD system.

Table 3 Dead state conditions for exergy analysis.

Parameter	Value
t_0 (°C)	15
P_0 (Pa)	101325
RH_0 (%)	50
$Sl_{sw,0}$ $(g\ kg^{-1})$	35
$\omega_0 \left(\dfrac{kg}{kg}\right)$	0.0053

4. Results and discussion

4.1 Model validation

The data taken from the experimental setup built by Idalex Inc. (USA) which is situated at the Gas Technology Institute Laboratory (USA) [31] is used to validate the exergy model of M-cycle based OAOW HDD system. The experimental setup was established to examine the idea of using the indirect dew point cooler for waste water distillation. This setup was made up of three adjacent air channels i.e., dry, evaporating, and condensing channels.

The current proposed system works along the same concept as the experimental setup. Therefore, the current model is validated using data from the experimental unit. The salinity of the waste water was not mentioned in the paper, so it was assumed as brackish water with 10 g/kg salinity [34] since water with added food color was taken as waste water in the experiment. Table 4 compares the present model with the results of the experiment [31]. The maximum absolute relative error was found to be 6.1%.

Table 4 Validation of current model with experimental results [31].

Parameter	Current model	Experimental [31]	Absolute relative error (%)
m_a $(kg\ h^{-1})$	532.6	532.6	-
t_1 (°C)	26.11	26.11	-
RH_1 (%)	69	69	-
m_{sw} $(kg\ h^{-1})$	68.04	68.04	-
Sl_{sw} $(g\ kg^{-1})$	10	-	-
MFRR	0.1278	0.1278	-
t_7 (°C)	60	60	-
t_3 (°C)	43.794	46.11	5.02
RH_3 (%)	100	100	-
m_{dw} $(kg\ h^{-1})$	20.692	19.5	6.1
RR	0.304	0.287	5.9

4.2 Effect of inlet air temperature to the M-cycle based HDD system

The outcome of numerical simulations for various inlet air temperatures to the M-cycle is discussed in this section. The inlet air temperatures are varied from 25 °C to 45 °C at a constant 10 g/kg of inlet air humidity ratio. The range of mass flow rate ratio (MFRR) is taken from 0.1 to 0.2 with the constant mass flow rate of the saline water at 100 kg/h. The inlet preheated saline water temperature to the M-cycle is taken as 60 °C and the inlet salinity of the saline water is taken as 35 g/kg. The heat supplied to the saline water heater is kept constant.
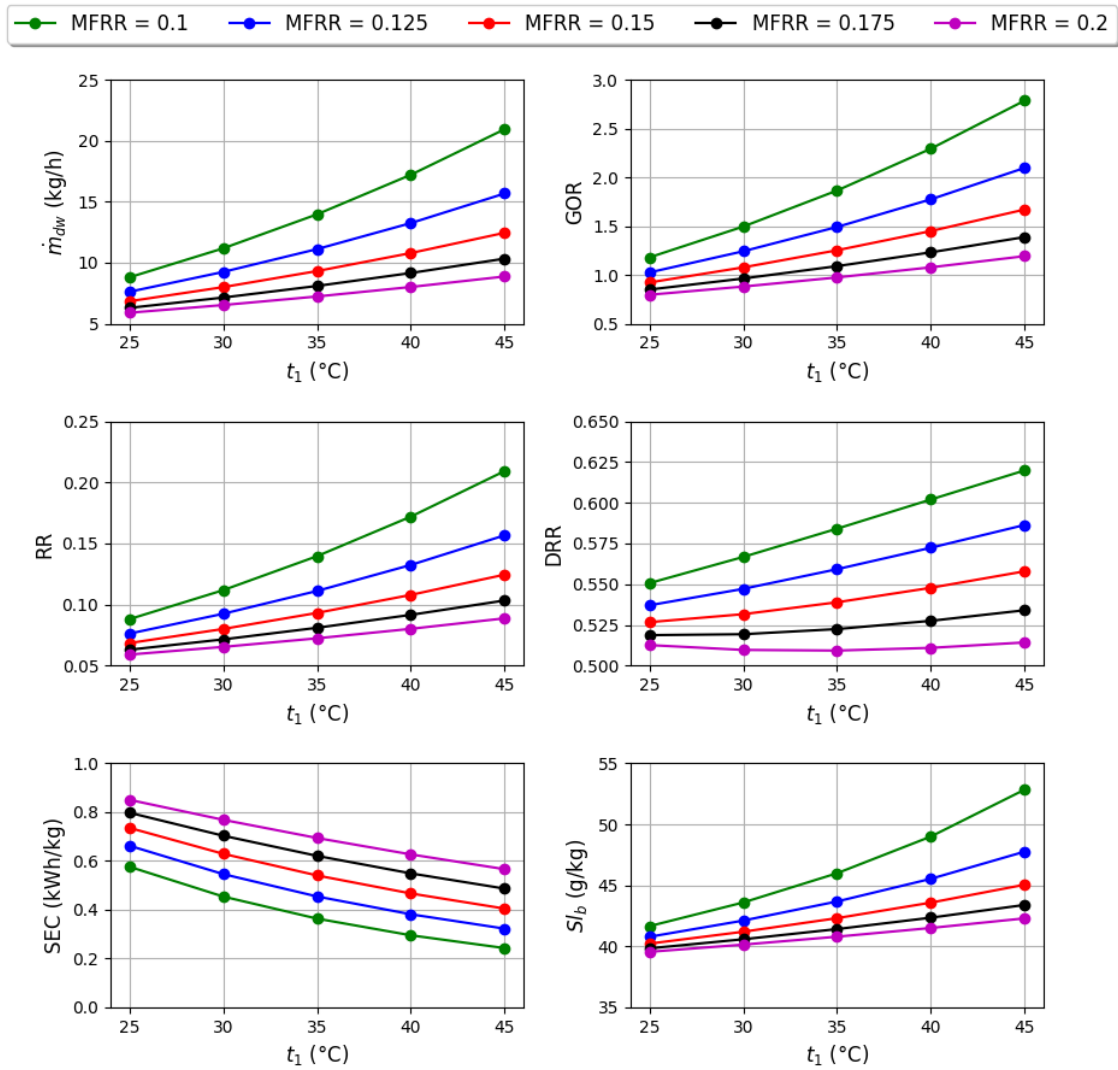
Figure 5 Effect of MFRR with various inlet air temperatures for different parameters; (i) mass flowrate of desalinated water (top left), (ii) Gain Output Ratio (top right), (iii) recovery ratio (middle left), (iv) desalination rate ratio (middle right), (v) specific energy consumption (bottom left) and (vi) brine salinity (bottom right).

Figure 5 illustrates the effect of MFRR on the energetic performance of the system at various inlet air temperatures. The mass flowrate of the desalinated water is decreasing with increase in MFRR for a specified temperature. The same trend is observed for a specific MFRR as air inlet temperature declines. The Gain

Output Ratio, recovery ratio, and brine salinity also follows the same characteristics as the mass flowrate of desalinated water with 2.81 and 0.212 as the maximum GOR, and RR respectively, for 21.2 kg/h of desalinated water at inlet air temperature of 45 °C and 0.1 MFRR. The specific energy consumption shows the opposite trend to the other performance parameters with the maximum being almost 0.85 kWh/kg at 0.2 MFRR and 25 °C inlet air temperature and minimum of around 0.25 kWh/kg at 0.1 MFRR and 45 °C inlet air temperature.
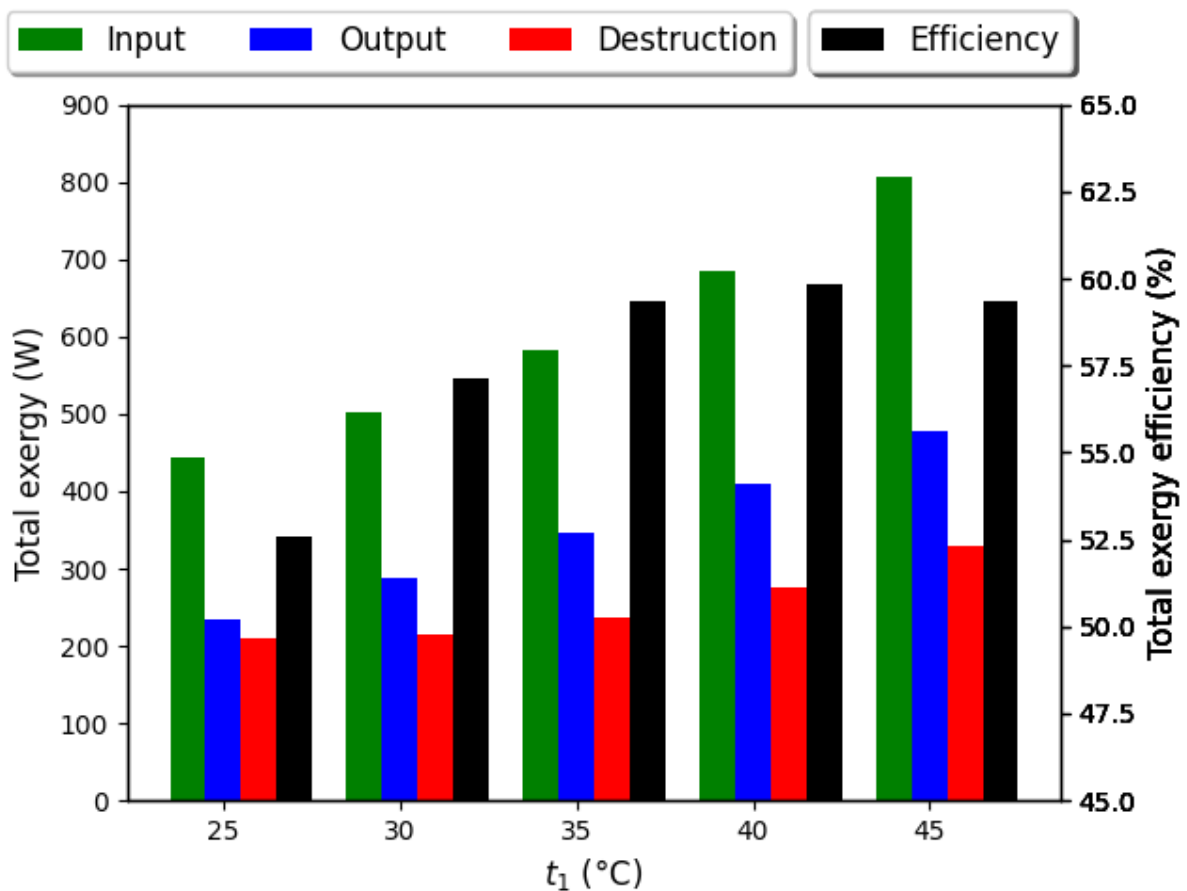
Figure 6 Variation of total exergy input, output, destruction, and efficiency with inlet air temperature at constant inlet air humidity ratio.

Figure 6 shows the total exergy input, output, destruction and efficiency for different inlet air temperatures at the constant inlet air humidity ratio and 0.1 MFRR. It is observed that there is a steady rise in both total exergy input and output with increase in the inlet temperature. It is noted that the exergy destruction

22

is almost same from 25 °C to 35 °C with a slight raise at 45 °C. When the temperature of inlet air is raised from 25 °C to 35 °C, an increasing trend in the total exergy efficiency, from 52.5 % to 60 %, is noted and then it remains almost constant with a slight decrease at 45 °C.

4.3 Effect of inlet air humidity ratio to the M-cycle based HDD system

The outcome of numerical simulations for various inlet air humidity ratios to the M-cycle is discussed in this section. The inlet air humidity ratio is ranged from 5 g/kg to 25 g/kg at a constant inlet air temperature of 45 °C. The MFRR is varied from 0.1 to 0.2 with the constant mass flow rate of the saline water at 100 kg/h. The inlet preheated saline water temperature to the M-cycle is taken as 60 °C and the salinity of the inlet saline water is taken as 35 g/kg. The heat supplied to the saline water heater is kept constant. Figure 7 presents the effect of MFRR on the energetic performance of the system at varying inlet air humidity ratios. While a steady decline is observed in the mass flow rate of the desalinated water, the GOR, recovery ratio, and the brine salinity with the rise in MFRR for a specific inlet air humidity ratio, they also decrease as the humidity ratio increases for a particular MFRR. The peak GOR of approximately 3 and RR of 0.223 are recorded for 22.3 kg/h desalinated water at 5 g/kg of inlet air humidity ratio and 0.1 MFRR. The specific energy consumption, as expected, follows the opposite behavior to the other previous parameters, with highest SEC of 0.7 kWh/kg at 0.2 MFRR and 25 g/kg inlet air humidity ratio and lowest SEC of 0.23 kWh/kg being achieved at 0.1 MFRR and 5 g/kg inlet air humidity ratio.
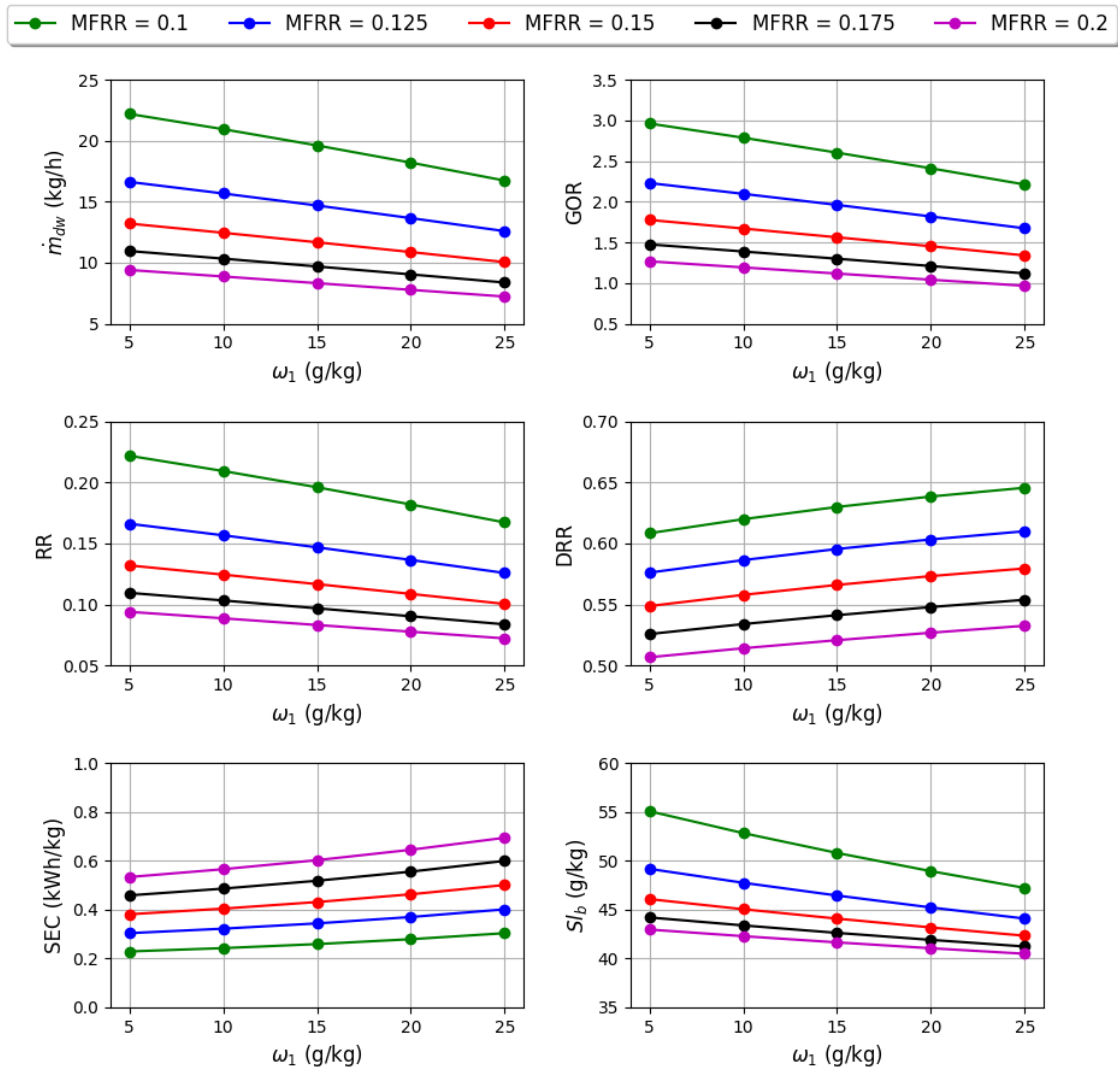
Figure 7 Effect of MFRR with various inlet air humidity ratios for different parameters; (i) mass flowrate of desalinated water (top left), (ii) Gain Output Ratio (top right), (iii) recovery ratio (middle left), (iv) desalination rate ratio (middle right), (v) specific energy consumption (bottom left) and (vi) brine salinity (bottom right).

Figure 8 presents the total exergy input, output, destruction and efficiency for different inlet air humidity ratios at constant inlet air temperature and 0.1 MFRR. The rise in the inlet air humidity ratio heightens the total exergy input with only a minute raise observed from 5 g/kg to 10 g/kg of inlet air humidity ratio. The

total exergy output increases uniformly when the humidity ratio of inlet air is increased. A fall in the total exergy destruction improves the total exergy efficiency from around 43 % to 85 %.
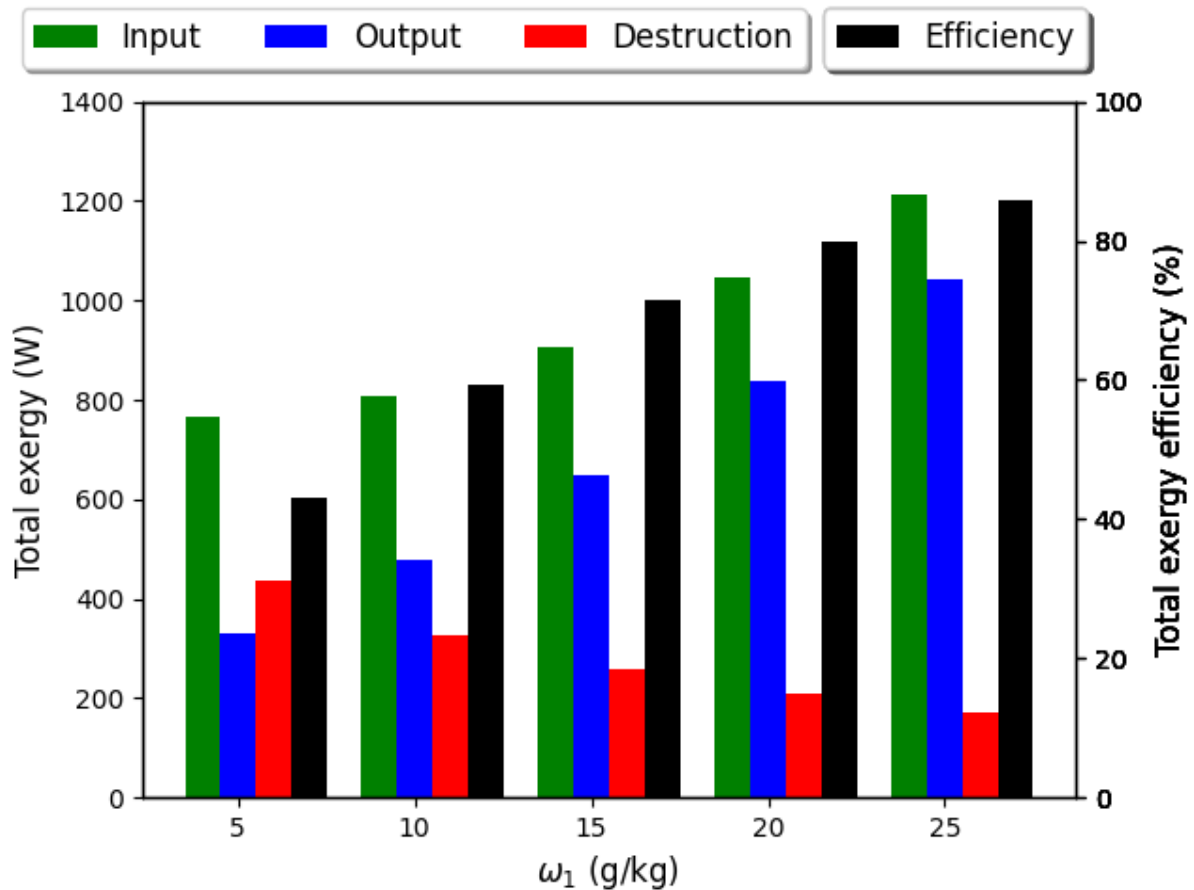
Figure 8 Variation of total exergy input, output, destruction, and efficiency with inlet air humidity ratio at constant inlet temperature.

4.4 Effect of inlet preheated saline water temperature to the M-cycle based HDD system

The outcome of numerical simulations for various temperatures of the inlet saline water to the M-cycle is discussed in this section. The range of the temperature of inlet preheated saline water is taken from 40 °C to 60 °C with the constant temperature of inlet air being 45 °C and the constant humidity ratio of inlet air being 10 g/kg. The MFRR is varied from 0.1 to 0.2 at 1000 kg/h of constant mass flow rate of air. The inlet salinity is 35 g/kg.

Figure 9 depicts the effect of MFRR on the energetic performance of the system at various inlet pre-heated saline water temperatures. At a specific temperature, the mass flow rate of desalinated water decreases with MFRR, and as the inlet pre-heated saline water temperature rises, greater mass flow rate of desalinated water is noted. At 0.1 MFRR, although the maximum GOR of about 4 is observed at a temperature of 40 °C, the highest recovery ratio of 0.211 is achieved at a temperature of 60 °C. The heat input values to the saline water heater and specific energy consumption follow a similar drift with both increasing as temperature and MFRR increase. The minimum SEC of 0.171 kWh/kg is observed at 0.1 MFRR and inlet pre-heated saline water temperature of 40 °C. Higher GOR is attained because of the lower heat supplied at the lower mass flow rate ratio.

Figure 10 illustrates the total exergy input, output, destruction and efficiency for different inlet pre-heated saline water temperatures at constant inlet salinity and 0.1 MFRR. When the inlet pre-heated saline water temperature increases, the total exergy input heightens steadily due to the larger heat input supplied to saline water heater. The total exergy output and destruction almost remain constant, showing minute increase with inlet pre-heated saline water temperature, as opposed to total exergy efficiency which falls from 46.8 % to 43.9 %.
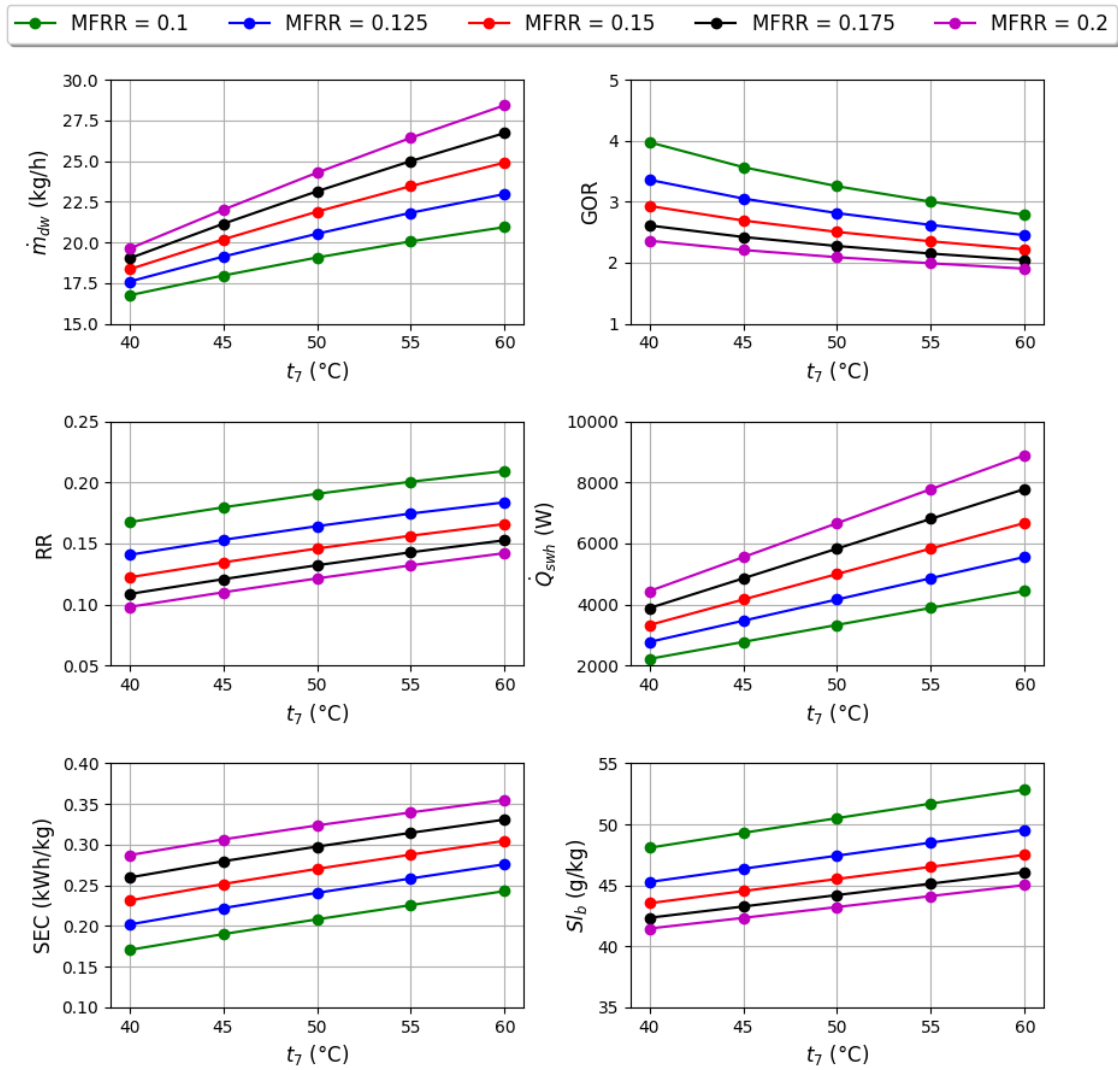
Figure 9 Effect of MFRR with various inlet pre-heated saline water temperatures for different parameters; (i) mass flowrate of desalinated water (top left), (ii) Gain Output Ratio (top right), (iii) recovery ratio (middle left), (iv) heat input to saline water heater (middle right), (v) specific energy consumption (bottom left) and (vi) brine salinity (bottom right).
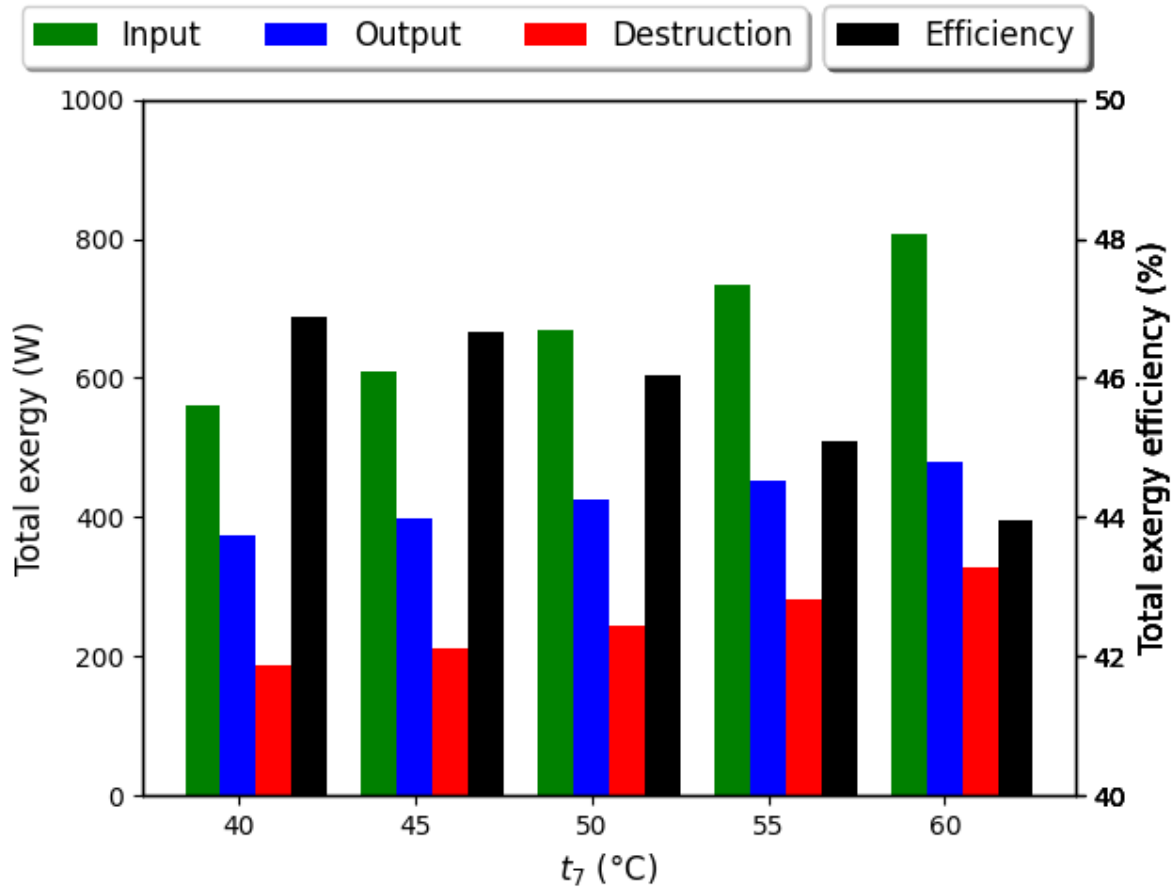
Figure 10 Variation of total exergy input, output, destruction, and efficiency with inlet pre-heated saline water temperatures at constant inlet salinity.

4.5 Effect of inlet salinity to the M-cycle based HDD system

The outcome of numerical simulations for various inlet salinities to the M-cycle is discussed in this section. The range of inlet salinity is from 10 g/kg to 50 g/kg at constant temperature of inlet preheated saline water as 60 °C. The mass flow rate of saline water is taken as 100 kg/h with MFRR equal to 0.1, temperature of inlet air being 45 °C and humidity ratio of inlet air being 10 g/kg.

Figure 11 shows the effect of inlet salinity on exergetic performance. With rise in inlet salinity, the exergy destruction declines and exergy efficiency improves from 43.2 % to 46%. This trend has been seen in other types of desalination systems like electrodialysis desalination [35].
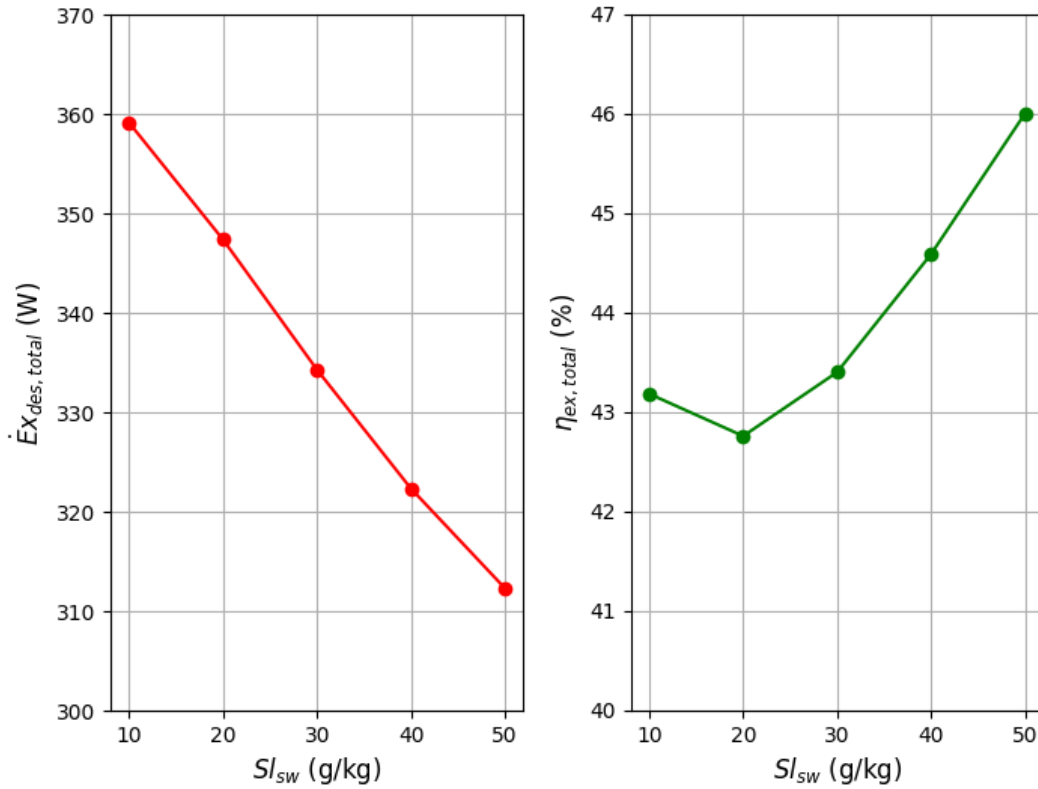
Figure 11 Effect of inlet salinity for different exergy parameters; (a) total exergy destruction (left), and (b) total exergy efficiency (right) with constant mass flow rate ratio.

4.6 Exergetic performance of different components

The exergetic performance of different components is discussed in this section. The MFRR is taken as 0.1, the temperature of inlet air is 45 °C, the humidity ratio of inlet air is 10 g/kg, inlet preheated saline water temperature to the M-cycle is taken as 60 °C, and inlet salinity is taken as 35 g/kg. Figure 12 represents the understanding of exergetic performance for the individual components as well as the complete system. The saline water heater is found to destroy the least exergy which intensifies its exergetic efficiency. In comparison, the M-cycle has the highest exergy destruction which lowers its exergetic efficiency. Since the

exergetic efficiency of the saline water heater is slightly less than 100 %, the exergetic efficiency of the whole system is marginally smaller than that of the M-cycle.
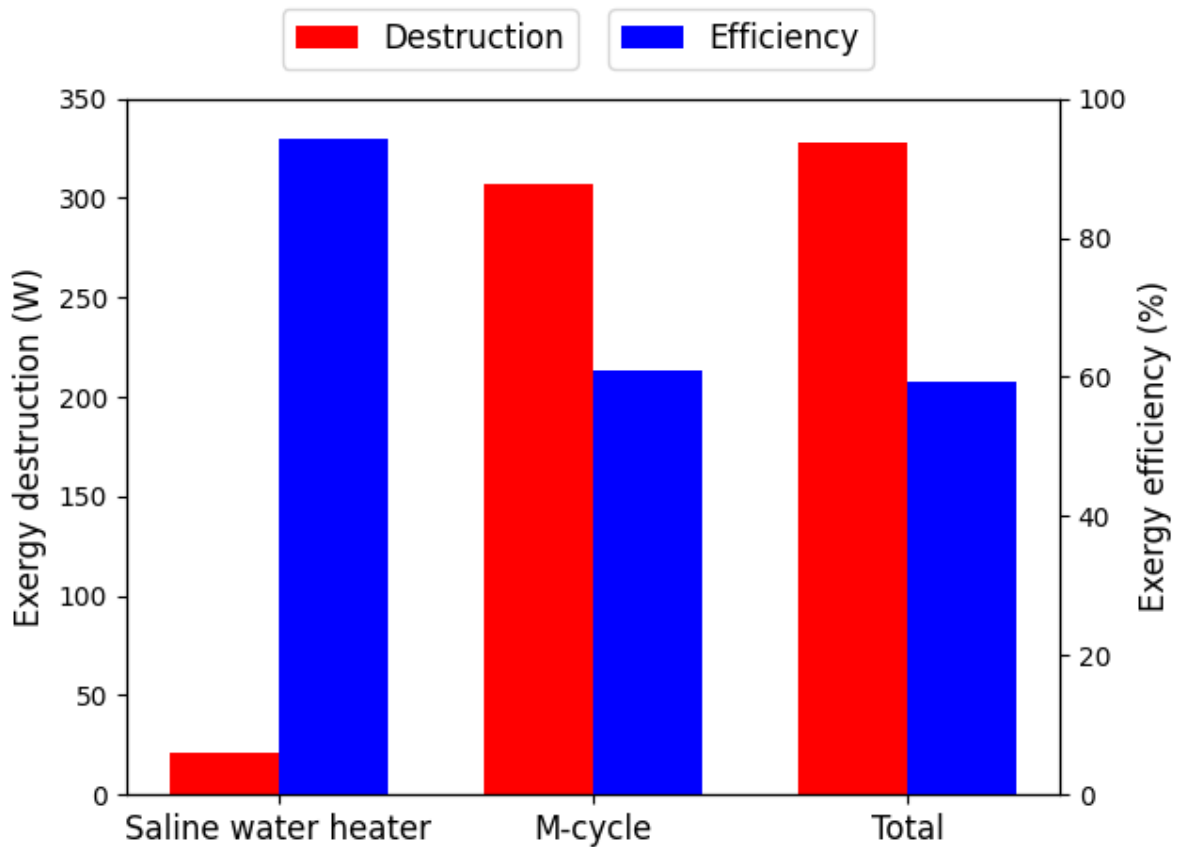
Figure 12 Variation of the exergy destruction and efficiency in each component for M-cycle based HDD system.

4.7 Total exergy balances

Figure 13 illustrates the graphical exergy flow diagram for M-cycle based HDD system. The Sankey diagram is a graphical technique identified as a useful tool for the exergy analysis [36]. All the exergy inputs, outputs and destruction values shown in Figure 13 are for the following conditions: 0.1 mass flow rate ratio, 45 °C and 10 g/kg inlet air temperature and humidity ratio respectively, 60 °C inlet preheated saline water temperature, and 35 g/kg inlet salinity. The heat supplied to the saline water heater and inlet air flow to the M-cycle are the two significant

contributors to the exergy input whereas the inlet saline water flow to the saline water heater has negligible effect on the exergy input. The major exergy output is due to exhaust air flow. In contrast, the effect on exergy output due to brine flow and desalinated water flow is to a lesser degree. The exergy destruction is 40.67 % of the total exergy input which results in an exergetic efficiency of 59.33 %.

Due to brine flow (3.01 %): 24.28 W
Due to heat supplied (44.04 %): 355.22 W
Due to exhaust air flow (53.72 %): 433.29 W
Input: 806.64 W
Due to inlet air flow (55.56 %): 448.20 W
Due to desalinated water flow (2.6 %): 20.99 W
Destruction (40.67 %): 328.08 W
Due to inlet saline water flow (0.4 %): 3.22 W
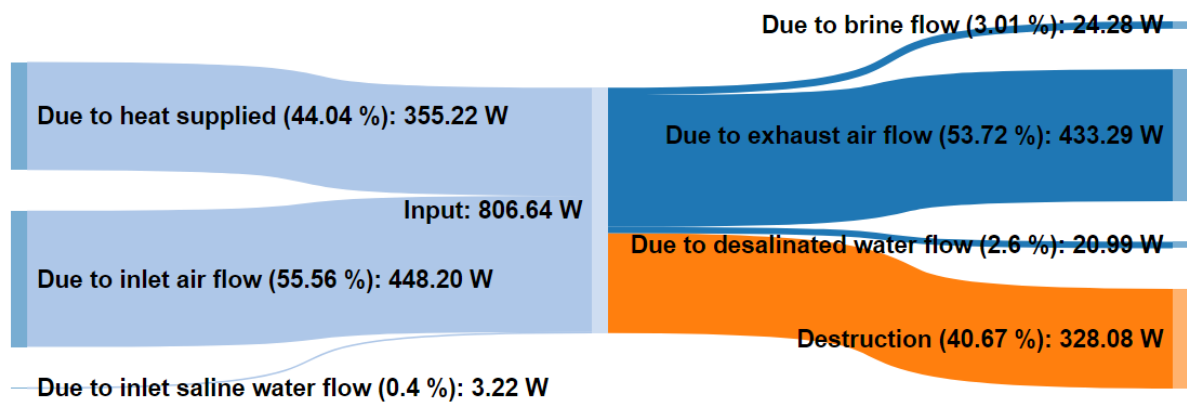
Figure 13 Graphical exergy flow diagram for M-cycle based HDD system.

4.8 Comparison with previous studies

The current study has shown the energetic and exergetic performance of the M-cycle based HDD system under a broad set of operating conditions. Table 5 outlines the contrast between the current M-cycle based HDD system and other integrated HDD systems based on different parameters like GOR and yield. Table 6 presents the difference between current open air open water M-cycle based HDD model and previous OAOW HDD system in terms of MFRR, mass flow rate of desalinated water, Gain Output Ratio, specific energy consumption and total entropy generation rate. A thermodynamic study of a water-heated OAOW HDD system with a packed-bed humidifier and dehumidifier investigated by He et al. [22] revealed that the maximum yield of 96.45 kg/h occurs at GOR of 1.7, SEC of 0.38 kWh/kg and with the total entropy generation rate of 85.73 W/K. The current model has also been studied for the thermodynamic performance and it has been inferred that 22.3 kg/h is the maximum mass flow rate of desalinated

water which takes place at a GOR of 3, SEC of 0.23 kWh/kg and the total entropy generation rate of 1.51 W/K. The present system performance is better than that of He et al., although the mass flow rate of freshwater is less due to lower MFRR.

Table 5 Comparison between the current M-cycle based HDD system and other integrated HDD systems from the literature.

Study	Research technique	Integrated system	GOR	Yield
Chen et al. [28]	Experiment, simulation	Indirect evaporative cooler	2.5	125 L/h
Faegh et al. [37]	Simulation	Vapor compression heat pump	2.47	0.91 kg/h
Chiranjeevi et al. [38]	Experiment, simulation	Vapor absorption refrigerator	1.53	2.2 kg/h
Lawal et al. [39]	Experiment	Vapor compression refrigerator	4.07	287.8 L/day
Xu et al. [40]	Experiment	Vapor compression heat pump	1.93	17.45 kg/h
Present study	Simulation	M-cycle	3	22.3 kg/h

Table 6 Comparison between current OAOW M-cycle based HDD model and previous OAOW HDD system from the literature.

Parameter	Current Model	He et al. [22]
$MFRR$	0.1 - 0.2	1.0 - 4.4
m_{dw} $(kg\ h^{-1})$	22.3	96.45
GOR	3	1.7
SEC $(kWh\ kg^{-1})$	0.23	0.38
$\dot{S}_{gen,total}$ $(W\ K^{-1})$	1.51	85.73

5. Conclusions

This paper focused on the comprehensive investigation of a water-heated open air open water (OAOW) HDD system that utilizes the vital water evaporation process of the Maisotsenko cycle (M-cycle). The energetic and exergetic performance were evaluated for various operating conditions. The employed M-cycle was composed of three types of air channels i.e., dry, humidification, and dehumidification channels respectively. A thermodynamic model of the proposed system was developed on the basis of the first and second law of thermodynamics. Following this, significant performance parameters, namely, recovery ratio (RR), Gain Output Ratio (GOR), specific energy consumption (SEC), exergy destruction, and exergy efficiency were analyzed. The concluding remarks yielded from the analysis are as follows:

1. It is observed for a specific inlet air temperature, that higher mass flow rate of air with constant mass flow rate of saline water enhances the mass flow rate of desalinated water and recovery ratio. In contrast, increasing mass flow rate of the saline water with a fixed mass flow rate of air increases the mass flow rate of the desalinated water but reduces the recovery ratio.

2. At a constant humidity ratio, an improvement in GOR is obtained with the rise in temperature of inlet air as well as mass flow rate of air while keeping the mass flow rate of saline water is kept constant. This is due to the greater desalinated water mass flow rate and constant heat supplied to the saline water heater. An air heater can be employed to boost the inlet air temperature, which in turn, maximizes the mass flow rate of desalinated water, but the inclusion of another component may lower the system performance.

3. As humidity ratio is elevated, at a certain inlet air temperature and MFRR, mass flow rate of desalinated water, GOR, RR, and rate of exergy destruction decline. This may be caused by addition of water content in the air entering the dry channel and it also confirms that the system can have lower performance but higher exergy efficiency. This reveals that the system works better in dry air ambient conditions than in humid air ambient conditions.

4. The Gain Output Ratio and specific energy consumption show the opposite trend for all the cases discussed.

5. For a particular inlet air temperature, it is observed that as the inlet preheated saline water temperature is heightened, the Gain Output Ratio drops and the rate of exergy destruction grows which results in reduced exergy efficiency.

6. An increase in inlet salinity, diminishes the exergy destruction and boosts the exergy efficiency. This may be due to added salt content in saline water.

7. The M-cycle has the utmost exergy destruction whereas the saline water heater is the least destroyed component. The maximum mass flow rate of desalinated water is 22.3 kg/h which occurs at 45 °C inlet air temperature, 5 g/kg humidity ratio, 60 °C pre-heated inlet saline water temperature, and

35 g/kg inlet salinity having GOR 3, SEC 0.23 kWh/kg, and exergy efficiency was found to be 43.2 %.

8. Based on the second law analysis, although the efficiency of the M-cycle based HDD system improves at higher ambient air temperature and humidity ratio, the system performs best within a temperature range of 35 °C to 45 °C and humidity ratio range of 15 g/kg to 25 g/kg.

Appendix

Thermodynamics properties of humid air have been taken from CoolProp [41] and ASHRAE fundamentals handbook [42]. But for flow exergy of humid air, the following equations have been used [43].

$$e_a = (h_a - h_0) - T_0(s_a - s_0) + RT_0\left(x_a \ln\frac{x_a}{x_{0,a}} + x_v \ln\frac{x_v}{x_{0,v}}\right) \qquad (A1)$$

$$x_a = \frac{1}{1+\omega} \qquad (A2)$$

$$x_v = \frac{\omega}{1+\omega} \qquad (A3)$$

Thermodynamic properties of saline water taken from literature [44–47].

$$\begin{aligned} h_{sw} = h_w - w_s(b_1 + b_2 w_s + b_3 w_s^2 + b_4 w_s^3 + b_5 T + b_6 T^2 + \\ b_7 T^3 + b_8 w_s T + b_9 w_s^2 T + b_{10} w_s T^2) \end{aligned} \qquad (A4)$$

$$h_w = 141.355 + 4202.070T - 0.535T^2 + 0.004T^3 \qquad (A5)$$

where,

$b_1 = -0.2348 \times 10^5, b_2 = 0.3152 \times 10^6, b_3 = 0.2803 \times 10^7,$

$b_4 = -0.1446 \times 10^8, b_5 = 0.7826 \times 10^4, b_6 = -0.4417 \times 10^2,$

$b_7 = 0.2139, b_8 = -0.1991 \times 10^5, b_9 = 0.2778 \times 10^5,$

$b_{10} = 0.9728 \times 10^2$

$$s_{sw} = s_w - w_s(c_1 + c_2 w_s + c_3 w_s^2 + c_4 w_s^3 + c_5 T + c_6 T^2 + c_7 T^3 + c_8 w_s T + c_9 w_s^2 T + c_{10} w_s T^2) \tag{A6}$$

$$s_w = 0.1543 + 15.383T - 2.996 \ x \ 10^{-2} T^2 + 8.193 \ x \ 10^{-5} T^3 - 1.370 \ x \ 10^{-7} T^4 \tag{A7}$$

where,

$c_1 = -0.4231 \times 10^3, c_2 = 0.1463 \times 10^5, c_3 = -0.9880 \times 10^5,$

$c_4 = 0.3095 \times 10^6, c_5 = 0.2562 \times 10^2, c_6 = -0.1443,$

$c_7 = 0.5879 \times 10^{-3}, c_8 = -0.6111 \times 10^2, c_9 = 0.8041 \times 10^2,$

$c_{10} = 0.3035$

$$\mu_w = \frac{\partial G_{sw}}{\partial m_w} = g_{sw} - w_s \frac{\partial g_{sw}}{\partial w_s} \tag{A8}$$

$$\mu_s = \frac{\partial G_{sw}}{\partial m_s} = g_{sw} + (1 - w_s) \frac{\partial g_{sw}}{\partial w_s} \tag{A9}$$

$$g_{sw} = h_{sw} - (T + 273.15)s_{sw} \tag{A10}$$

$$\frac{\partial g_{sw}}{\partial w_s} = \frac{\partial h_{sw}}{\partial w_s} - (T + 273.15)\frac{\partial s}{\partial w_s} \tag{A11}$$

$$-\frac{\partial h_{sw}}{\partial w_s} = b_1 + 2b_2 w_s + 3b_3 w_s^2 + 4b_4 w_s^3 + b_5 T + b_6 T^2 + b_7 T^3 + 2b_8 w_s T + 3b_9 w_s^2 T + 2b_{10} w_s T^2 \tag{A12}$$

$$-\frac{\partial s_{sw}}{\partial w_s} = c_1 + 2c_2 w_s + 3c_3 w_s^2 + 4c_4 w_s^3 + c_5 T + c_6 T^2 + c_7 T^3 + 2c_8 w_s T + 3c_9 w_s^2 T + 2c_{10} w_s T^2 \tag{A13}$$

References

[1] S. Kumar Nougriaya, M.K. Chopra, B. Gupta, P. Baredar, Stepped solar still: A review on designs analysis, Materials Today: Proceedings. (2020). https://doi.org/10.1016/j.matpr.2020.09.598.

[2] D.U. Lawal, N.A.A. Qasem, Humidification-dehumidification desalination systems driven by thermal-based renewable and low-grade energy sources: A critical review, Renew. Sustain. Energy Rev. 125 (2020) 109817. https://doi.org/10.1016/j.rser.2020.109817.

[3] M. Faegh, P. Behnam, M.B. Shafii, A review on recent advances in humidification-dehumidification (HDH) desalination systems integrated with refrigeration, power and desalination technologies, Energy Convers. Manage. 196 (2019) 1002–1036. https://doi.org/10.1016/j.enconman.2019.06.063.

[4] A. Eghtesad, M. Salakhi, H. Afshin, S.K. Hannani, Numerical investigation and optimization of indirect freeze desalination, Desalination. 481 (2020) 114378. https://doi.org/10.1016/j.desal.2020.114378.

[5] M. Asadollahi, D. Bastani, S.A. Musavi, Enhancement of surface properties and performance of reverse osmosis membranes after surface modification: A review, Desalination. 420 (2017) 330–383. https://doi.org/10.1016/j.desal.2017.05.027.

[6] F. Alnaimat, M. Ziauddin, B. Mathew, A review of recent advances in humidification and dehumidification desalination technologies using solar energy, Desalination. 499 (2021) 114860. https://doi.org/10.1016/j.desal.2020.114860.

[7] G.P. Narayan, M.H. Sharqawy, E.K. Summers, J.H. Lienhard, S.M. Zubair, M.A. Antar, The potential of solar-driven humidification–dehumidification desalination for small-scale decentralized water production, Renewable Sustainable Energy Rev. 14 (2010) 1187–1201. https://doi.org/10.1016/j.rser.2009.11.014.

[8] M.S. Elzayed, M.A.M. Ahmed, M.A. Antar, M.H. Sharqawy, S.M. Zubair, The impact of thermodynamic balancing on the performance of a humidification dehumidification desalination system, Therm. Sci. Eng. Prog. 21 (2021) 100794. https://doi.org/10.1016/j.tsep.2020.100794.

[9] W.F. He, D. Han, W.P. Zhu, C. Ji, Thermo-economic analysis of a water-heated humidification-dehumidification desalination system with waste heat recovery, Energy Convers. Manage. 160 (2018) 182–190. https://doi.org/10.1016/j.enconman.2018.01.048.

[10] W.F. He, L.N. Xu, D. Han, L. Gao, Performance analysis of an air-heated humidification–dehumidification desalination plant powered by low grade waste heat, Energy Convers. Manage. 118 (2016) 12–20. https://doi.org/10.1016/j.enconman.2016.03.073.

[11] A. Khalil, S.A. El-Agouz, Y.A.F. El-Samadony, A. Abdo, Solar water desalination using an air bubble column humidifier, Desalination. 372 (2015) 7–16. https://doi.org/10.1016/j.desal.2015.06.010.

[12] H.M. Abd-ur-Rehman, F.A. Al-Sulaiman, A novel design of a multistage stepped bubble column humidifier for the humidification of air, Appl. Therm. Eng. 120 (2017) 530–536. https://doi.org/10.1016/j.applthermaleng.2017.04.021.

[13] G. Prakash Narayan, M.G. St. John, S.M. Zubair, J.H. Lienhard, Thermal design of the humidification dehumidification desalination system: An experimental investigation, Int. J. Heat Mass Transf. 58 (2013) 740–748. https://doi.org/10.1016/j.ijheatmasstransfer.2012.11.035.

[14] Z. Rahimi-Ahar, M.S. Hatamipour, Y. Ghalavand, Experimental investigation of a solar vacuum humidification-dehumidification (VHDH) desalination system, Desalination. 437 (2018) 73–80. https://doi.org/10.1016/j.desal.2018.03.002.

[15] A.E. Kabeel, M. Abdelgaied, Experimental evaluation of a two-stage indirect solar dryer with reheating coupled with HDH desalination system

for remote areas, Desalination. 425 (2018) 22–29.
https://doi.org/10.1016/j.desal.2017.10.016.

[16] S.M. Zubair, M.A. Antar, S.M. Elmutasim, D.U. Lawal, Performance evaluation of humidification-dehumidification (HDH) desalination systems with and without heat recovery options: An experimental and theoretical investigation, Desalination. 436 (2018) 161–175. https://doi.org/10.1016/j.desal.2018.02.018.

[17] P. Behnam, M.B. Shafii, Examination of a solar desalination system equipped with an air bubble column humidifier, evacuated tube collectors and thermosyphon heat pipes, Desalination. 397 (2016) 30–37. https://doi.org/10.1016/j.desal.2016.06.016.

[18] A.S. Nafey, H.E.S. Fath, S.O. El-Helaby, A. Soliman, Solar desalination using humidification–dehumidification processes. Part II. An experimental investigation, Energy Convers. Manage. 45 (2004) 1263–1277. https://doi.org/10.1016/S0196-8904(03)00152-3.

[19] G.P. Narayan, M.H. Sharqawy, J.H. Lienhard V., S.M. Zubair, Thermodynamic analysis of humidification dehumidification desalination cycles, Desalination Water Treat. 16 (2010) 339–353. https://doi.org/10.5004/dwt.2010.1078.

[20] K.H. Mistry, J.H. Lienhard, S.M. Zubair, Effect of entropy generation on the performance of humidification-dehumidification desalination cycles, Int. J. Therm. Sci. 49 (2010) 1837–1847. https://doi.org/10.1016/j.ijthermalsci.2010.05.002.

[21] K.H. Mistry, A. Mitsos, J.H. Lienhard, Optimal operating conditions and configurations for humidification–dehumidification desalination cycles, Int. J. Therm. Sci. 50 (2011) 779–789. https://doi.org/10.1016/j.ijthermalsci.2010.12.013.

[22] W.F. He, J.J. Chen, D. Han, L.T. Luo, X.C. Wang, Q.Y. Zhang, S.Y. Yao, Energetic, entropic and economic analysis of an open-air, open-water

humidification dehumidification desalination system with a packing bed dehumidifier, Energy Convers. Manage. 199 (2019) 112016. https://doi.org/10.1016/j.enconman.2019.112016.

[23] H. Xu, X.Y. Sun, Y.J. Dai, Thermodynamic study on an enhanced humidification-dehumidification solar desalination system with weakly compressed air and internal heat recovery, Energy Convers. Manage. 181 (2019) 68–79. https://doi.org/10.1016/j.enconman.2018.11.073.

[24] M.H. Mahmood, M. Sultan, T. Miyazaki, S. Koyama, V.S. Maisotsenko, Overview of the Maisotsenko cycle--A way towards dew point evaporative cooling, Renewable Sustainable Energy Rev. 66 (2016) 537–555. https://www.sciencedirect.com/science/article/pii/S1364032116304361.

[25] H. Sadighi Dizaji, E.J. Hu, L. Chen, S. Pourhedayat, Comprehensive exergetic study of regenerative Maisotsenko air cooler; formulation and sensitivity analysis, Appl. Therm. Eng. 152 (2019) 455–467. https://doi.org/10.1016/j.applthermaleng.2019.02.067.

[26] J. Lin, D.T. Bui, R. Wang, K.J. Chua, On the exergy analysis of the counter-flow dew point evaporative cooler, Energy. 165 (2018) 958–971. https://doi.org/10.1016/j.energy.2018.10.042.

[27] B. Porumb, P. Ungureşan, L.F. Tutunaru, A. Şerban, M. Bălan, A Review of Indirect Evaporative Cooling Technology, Energy Procedia. 85 (2016) 461–471. https://doi.org/10.1016/j.egypro.2015.12.228.

[28] Q. Chen, M. Burhan, M.W. Shahzad, D. Ybyraiymkul, F.H. Akhtar, K.C. Ng, Simultaneous production of cooling and freshwater by an integrated indirect evaporative cooling and humidification-dehumidification desalination cycle, Energy Convers. Manag. 221 (2020) 113169. https://doi.org/10.1016/j.enconman.2020.113169.

[29] R. Tariq, N.A. Sheikh, J. Xamán, A. Bassam, An innovative air saturator for humidification-dehumidification desalination application, Appl.

Energy. 228 (2018) 789–807.

https://doi.org/10.1016/j.apenergy.2018.06.135.

[30] D. Pandelidis, A. Cichoń, A. Pacak, P. Drąg, M. Drąg, W. Worek, S. Cetin, Water desalination through the dewpoint evaporative system, Energy Convers. Manag. 229 (2021) 113757.

https://doi.org/10.1016/j.enconman.2020.113757.

[31] Chudnovsky, Yaroslav; Aleksandr Kozlov (Gas Technology Institute). Integrated Industrial Wastewater Reuse Via Heat Recovery. California Energy Commission. 2014. Publication number: CEC-500-2015-049.

[32] B. Riangvilaikul, S. Kumar, Numerical study of a novel dew point evaporative cooling system, Energy Build. 42 (2010) 2241–2250. https://doi.org/10.1016/j.enbuild.2010.07.020.

[33] B.L. de O. Campos, A.O.S. da Costa, E.F. da Costa Junior, Mathematical modeling and sensibility analysis of a solar humidification-dehumidification desalination system considering saturated air, Solar Energy. 157 (2017) 321–327.

https://doi.org/10.1016/j.solener.2017.08.029.

[34] J.R. Du, X. Zhang, X. Feng, Y. Wu, F. Cheng, M.E.A. Ali, Desalination of high salinity brackish water by an NF-RO hybrid system, Desalination. 491 (2020) 114445. https://doi.org/10.1016/j.desal.2020.114445.

[35] M.M. Generous, N.A.A. Qasem, S.M. Zubair, Exergy-based entropy-generation analysis of electrodialysis desalination systems, Energy Convers. Manag. 220 (2020) 113119.

https://doi.org/10.1016/j.enconman.2020.113119.

[36] K. Soundararajan, H.K. Ho, B. Su, Sankey diagram framework for energy and exergy flows, Appl. Energy. 136 (2014) 1035–1042.

https://doi.org/10.1016/j.apenergy.2014.08.070.

[37] M. Faegh, M.B. Shafii, Performance evaluation of a novel compact humidification-dehumidification desalination system coupled with a heat

pump for design and off-design conditions, Energy Convers. Manage. 194 (2019) 160–172. https://doi.org/10.1016/j.enconman.2019.04.079.

[38] C. Chiranjeevi, T. Srinivas, Augmented desalination with cooling integration, Int. J. Refrig. 80 (2017) 106–119. https://doi.org/10.1016/j.ijrefrig.2017.05.007.

[39] D.U. Lawal, M.A. Antar, A. Khalifa, S.M. Zubair, F. Al-Sulaiman, Experimental investigation of heat pump driven humidification-dehumidification desalination system for water desalination and space conditioning, Desalination. 475 (2020) 114199. https://doi.org/10.1016/j.desal.2019.114199.

[40] H. Xu, Y. Zhao, Y.J. Dai, Experimental study on a solar assisted heat pump desalination unit with internal heat recovery based on humidification-dehumidification process, Desalination. 452 (2019) 247–257. https://doi.org/10.1016/j.desal.2018.11.019.

[41] I.H. Bell, J. Wronski, S. Quoilin, V. Lemort, Pure and Pseudo-pure Fluid Thermophysical Property Evaluation and the Open-Source Thermophysical Property Library CoolProp, Ind. Eng. Chem. Res. 53 (2014) 2498–2508. https://doi.org/10.1021/ie4033999.

[42] 2017 ASHRAE Handbook: Fundamentals, American Society of Heating Refrigerating and Air-Conditioning Engineers Incorporated, 2017. https://play.google.com/store/books/details?id=8HRatgEACAAJ.

[43] A. Bejan, Advanced Engineering Thermodynamics, John Wiley & Sons, 2016. https://play.google.com/store/books/details?id=j0zSDAAAQBAJ.

[44] K.G. Nayar, M.H. Sharqawy, L.D. Banchik, J.H. Lienhard V., Thermophysical properties of seawater: A review and new correlations that include pressure dependence, Desalination. 390 (2016) 1–24. https://doi.org/10.1016/j.desal.2016.02.024.

[45] M.H. Sharqawy, J.H. Lienhard V., S.M. Zubair, Thermophysical properties of seawater: a review of existing correlations and data, Desalination Water Treat. 16 (2010) 354–380. https://doi.org/10.5004/dwt.2010.1079.

[46] M.H. Sharqawy, J.H. Lienhard V., S.M. Zubair, On exergy calculations of seawater with applications in desalination systems, Int. J. Therm. Sci. 50 (2011) 187–196. https://doi.org/10.1016/j.ijthermalsci.2010.09.013.

[47] M.H. Sharqawy, S.M. Zubair, J.H. Lienhard, Second law analysis of reverse osmosis desalination plants: An alternative design using pressure retarded osmosis, Energy. 36 (2011) 6617–6626. https://doi.org/10.1016/j.energy.2011.08.056.

Declaration of interests

☒The authors declare that they have no known competing financial interests or personal relationships that could have appeared to influence the work reported in this paper.

☐The authors declare the following financial interests/personal relationships which may be considered as potential competing interests:

CRediT authorship contribution statement

Mansoor Abdul Aziz: Methodology, Software, Writing - Original draft preparation, Visualization.

Jie Lin: Writing - Review and Editing.

František Mikšík: Discussion, Supervision.

Takahiko Miyazaki: Conceptualization, Supervision.

Kyaw Thu: Conceptualization, Supervision, Writing - Review and Editing.